

## RESEARCH PAPER

# Effect of Zinc Oxide on Structural and Optical Properties Borotellurite Glass: Ternary Glass

Aso F.Mohamed<sup>1</sup>, Saman Q.Mawlud<sup>2</sup>

Department of physic, College of Education, Salahaddin University- Erbil, Kurdistan Region, Iraq

### ABSTRACT:

A series of zinc borotellurite glass with the composition of  $(70-x)\text{TeO}_2-30\text{B}_2\text{O}_3-x\text{ZnO}$  ( $0 \leq x \leq 20$ ) have been successfully synthesized by melt quenching techniques. Physical parameters such as density, molar volume and refractive index have been calculated, and maximum values of refractive index and density were obtained at 2.315 and 4.57, respectively. The amorphous nature of the glass sample was confirmed using the X-ray diffraction (XRD) technique; no sharp pick was observed in the XRD pattern, which confirms that the glass sample structure has amorphous nature. The absorption spectra were studied by using a UV-Vis-NIR spectrometer, and the values of direct band gap ( $E_{dir}$ ), indirect band gap ( $E_{ind}$ ) and Urbach energy ( $E_u$ ) were obtained through the absorption edge studies. It was found that the  $E_{dir}$  values were between 3.54 and 3.69 eV and the values of  $E_{ind}$  lies between 3.33 and 3.51 eV. The  $E_u$  values lie between 0.17 to 0.21 eV. The bonding parameters of the glasses were analyzed by using Fourier Transform Infrared (FTIR) technique, and the formation of non-bridging oxygen (NBO) was observed, which indicates the presence of  $\text{TeO}_4$ ,  $\text{BO}_3$  and  $\text{BO}_4$  units.

KEY WORDS: Zinc borotellurite , Physical properties, XRD, FTIR

DOI: <http://dx.doi.org/10.21271/ZJPAS.35.4.02>

ZJPAS (2023) , 35(4);14-21 .

### 1.INTRODUCTION :

Glasses are unique materials that have been used for thousands of years (Mawlud 2018). Important products like glass have cooled to a rigid state without crystallizing (Mekki, Khattak et al. 2005). Glass materials were developed rapidly in the 20th century because of their chemical, physical, mechanical, electrical, magnetic, and especially optical properties, which make it suitable for a wide range of applications in semiconductors, optoelectronic devices, storage devices, and reinforcement materials in science and industry. (El-Mallawany 2018).

One of the best glass hosts for scientific and technological interest is tellurium dioxide-based glass, which has advantageous characteristics like high dielectric constants, high refractive index, and low melting temperatures. It also exhibits good transparency in the visible and infrared regions (Kaur, Khanna et al. 2010).

One of the most attractive substances whose structural properties have received extensive research is borate. In borate crystals and glasses, the boron atom typically coordinates with three or four oxygen atoms to form structural units called  $\text{BO}_3$  or  $\text{BO}_4$ . (Saddeek, Gaafar et al. 2009). The degree of polymerization in a borate network is increased by the addition of a modifier oxide; as a result, the basic units switch from  $\text{BO}_3$  to  $\text{BO}_4$  and the boron coordination changes from trigonal to tetrahedral (Ardelean, Mureşan et al. 2007). Because of their scientific interest and useful

---

#### \* Corresponding Author:

Aso Farhan Mohamed

E-mail: [aso.mohamed@su.edu.krd](mailto:aso.mohamed@su.edu.krd)

#### Article History:

Received: 08/11/2022

Accepted: 27/12/2022

Published: 30/08 /2023

technological application, borotellurite glasses have drawn considerable attention and been the subject of extensive research (Kundu, Dhankhar et al. 2014). Science is interested in how tellurium oxide,  $\text{TeO}_2$ , and borate oxide,  $\text{B}_2\text{O}_3$ , combine to form borotellurite glass. Because  $\text{TeO}_2$  and  $\text{B}_2\text{O}_3$  are present in borotellurite glass, this may indicate complex glass structure specifications (Gautam and Yadav 2013).

The addition of glass modifiers such as zinc oxide (ZnO) into borotellurite glass lowers crystallisation rates (Pavani, Sadhana et al. 2011), and the addition of ZnO in glass structure produces a durable glass, reducing the melting point and increases the glass forming ability. It also enhance the glass's physical parameters, structural and optical properties (Hasnimulyati, Halimah et al. 2016). Due to the higher polarizability of the ions and lower melting temperature of the substance, zinc oxide doped borotellurite glasses with low melting points are of particular interest because of their applications in various fields of electronic products (El-Falaky, Guirguis et al. 2012).

In this research, our aim is to prepare a glass based on borotellurite doped with different mol% ratios of modifier zinc oxide by using a conventional melt quenching technique, the physical parameters of this glass and the glass properties in terms of optical and structural characteristics have been studied.

## 2. Glass Preparation

Tellurite glass with an appropriate composition ratio of  $(70-x)\text{TeO}_2-30\text{B}_2\text{O}_3-x\text{ZnO}$  where  $x=0,5,10,15$  and  $20$  mol% prepared by sign rapid melt quenching technique. All raw materials in powder form were provided by Sigma Aldrich company with a high purity of  $\text{TeO}_2(\geq 99\%)$ ,  $\text{B}_2\text{O}_3(\geq 98.0\%)$  and  $\text{ZnO}$  (99.9%). The raw materials with required proportions were weighted using a sensitive 6 digit electronic balance (Electronic Balance RADWAG AS 220-R1). The total weight of the constituents of all mixed composition as powders was approximately  $10\pm 0.001$  grams. A 10 gm of the chemical composition were mixed using an electric motor rotator and milled for 15 min to ensure the powders were homogenous. Then, the mixtures were poured into an alumina crucible and put it inside an electrical furnace at  $900^\circ\text{C}$  for 30 min for the melting process. After the composition fully melted and the desired viscosity was

achieved, the mixtures were immediately transferred to another furnace for the annealing process by pouring the melt on a brass mould for an annealing time 1h at  $350^\circ\text{C}$ . The furnace is then turned off and allowed to cool down gradually until it approaches room temperature. All the prepared glass samples were visually transparent and in yellowish colour. After that, the glass samples were prepared for the spectroscopic technique by polishing and graining until an appropriate thickness 2 mm was achieved with high transparency; on the other hand, the glass bulk was converted into fine powder for studying the structural characterization. Fig(1) shows the group of prepared samples. It was observed that all glasses' colours are yellowish.

The amorphous nature of the glass is confirmed by the Panalytical X' Pert Pro X-ray diffractometer. The measurement analyzed over  $2\theta = 20^\circ-80^\circ$ . The FTIR spectra were analyzed at room temperature between  $400-4000\text{ cm}^{-1}$  using Perkin Elmer Spectrum Two with the KBr pellet method. Meanwhile, UV-Vis-NIR spectrophotometer JASCO V-770 reported the optical absorption spectra of the glass samples in the range of 200 nm to 900 nm at room temperature. From the absorption spectra, values of direct and indirect optical band gaps and Urbach energy are calculated by using the Mott-Davis equation.



Fig. 1. Prepared glass sample

## 3. RESULTS AND DISCUSSIONS

### 3.1 Physical Properties, Energy Band Gap and Urbach Energy

The glass compositions, molecular weights, and glass labels for each reagent are listed in table (1). The physical properties of the prepared samples for the different ratios of ZnO are determined using a set of formulas referred to below. Density is a very significant for evaluating the degree of compactness in glassy system. The usual method of testing the compactness of glass materials is density (Mawlud 2021). The density ( $\rho$ ) for each sample is measured by the Archimedes method; the density of the glass samples is determined by the following equation :

$$\rho = \rho_d \left( \frac{W_a}{W_a - W_d} \right) \dots\dots 3.1$$

where  $W_a$  and  $W_d$  are the weight of the glass sample in the air and the distal water, respectively,  $\rho_d$  is the density of distal water. The molar volume is given by:

$$V_M = \frac{M_{ave}}{\rho} \dots\dots 3.2$$

Where  $\rho$  is the density of glass and  $M_{ave}$  is the average molecular weight of the glass is calculated by using the equation :

$$M_{ave} = \chi_{TeO_2}M_{TeO_2} + \chi_{B_2O_3}M_{B_2O_3} + \chi_{ZnO}M_{ZnO} \dots\dots 3.3$$

Where  $M_{Ox}$  and  $\chi_{Ox}$  are the molar mass and molar fraction of different oxides, respectively. The measured and calculated physical quantities are presented in table(1).

Figure 2 shows the ternary glassy phase diagram; the ratio of ingredients used to make the glass was in conformity with two previously published papers (Pavani, Sadhana et al. 2011) (Kumari, Yadav et al. 2021).

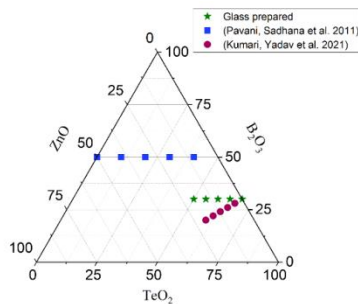


Fig.2. Ternary diagram for Zinc borotellurite glass composition  $(70 - x)TeO_2 - 30B_2O_3 - xZnO$

The physical properties of the glass samples are calculated using a set of equations (3.1), (3.2) and (3.3). The values of density ( $\rho$ ), average molecular weight ( $M_{ave}$ ) and molar volume ( $V_M$ ) of all glass samples are listed in the table (1). It is known that the density of a material is highly dependent on the molecular weight of the material. The variation of density and molar volume with the concentration of ZnO is shown in fig. (3). As anticipated, the addition of ZnO to the

borotellurite network results in some sort of atom structural rearrangement. The substitution of ZnO into the borotellurite glassy network raises the possibility of changing the geometrical configuration. The decrease in glass density is clearly indicated when the amount of ZnO increases from zero to 15 mol%, the reason reflecting the transformation of ZnO atoms to the host structure by breaking (Te-O) bonds and producing a large number of NBO, When the ZnO content increases to 20 mol% it causes an increase in density indicating that the zinc ions penetrate into the borotellurite glass network leading to higher BO content. (Sidek, Rosmawati et al. 2009). Contrary to the typical theoretical predictions that the density and molar volume have an inverse relationship (Sharma, Goswami et al. 2004). As more ZnO molecules are added to the glass as density, the molar volume is seen in Figure 3 below to be on the decline. This might be due to the fact that zinc's atomic size is smaller than those of tellurite and boric (Halimah, Umar et al. 2019). Additionally, Zn-O bond 's length is shorter than Te-O. As a result, more gaps are filled when more ZnO is added to borotellurite (Halimah, Umar et al. 2019).

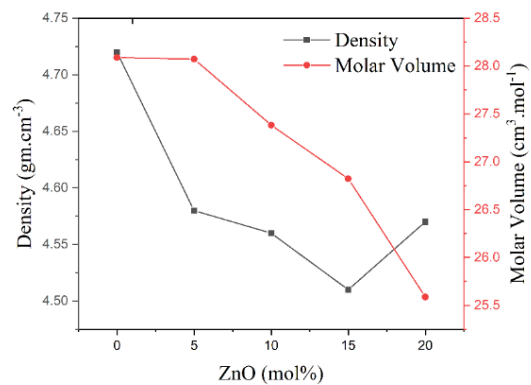


Fig. 3. Variation of Density and molar volume with ZnO concentration

Table 1. ZnO (mol%), Density ( $\rho, gm/cm^3$ ), molar volume ( $V_m, cm^3/mol$ ), Average molecular weight ( $M_{avg}, gm/mol$ ), direct band gap energy  $E_{dir}(eV)$ , indirect band gap energy  $E_{ind}(eV)$  and Urbach energy  $E_U(eV)$  of the proposed  $(70 - x)TeO_2 - 30B_2O_3 - xZnO$

Sample Code	ZnO	$\rho$	$V_M$	$M_{ave}$	$E_{dir}$	$E_{ind}$	$E_U$	$n$	Colour
TBZ 1	0	4.72	28.09	132.57	3.56	3.35	0.20	2.31	Light yellow
TBZ 2	5	4.58	28.07	128.56	3.57	3.36	0.17	2.30	Light yellow
TBZ 3	10	4.56	27.38	124.86	3.54	3.33	0.21	2.32	Yellow
TBZ 4	15	4.51	26.82	120.96	3.69	3.51	0.17	2.27	Yellow

TBZ 5	20	4.57	25.59	116.93	3.66	3.40	0.19	2.30	Dark yellow
-------	----	------	-------	--------	------	------	------	------	-------------

3.54 eV – 3.69 eV ) and (3.33 eV-3.51 eV), respectively (Ahmed, Ibrahim et al. 2017).

The disorder effect in the glass system can be used to explain the variation in refractive index. In fig.(4) the relationship between refractive index, density, and average molar mass is plotted . As ZnO concentration rises from 0 to 15 mol%, molar mass builds up and the refractive index gradually falls. This decrease is the result of TeO<sub>3</sub> in the glass network forming TeO<sub>3+1</sub> polyhedra. When ZnO was added further, up to 20 mol%, it was evident that BO was formed because the refractive index rose.

The analysis and determination of the prepared samples' energy band gap is one of the advantages of the UV-Vis-NIR spectrum. Due to the contribution of lattice vibrations (phonons), the indirect band gap is established by bridging the valence band–conduction band gap. When Davis and Mott first discussed the indirect band gap as:

$$\alpha(\omega) = \frac{\text{constant}(\hbar\omega - E_{opt})^n}{\hbar\omega} \dots\dots 3.4$$

Where  $\hbar\omega$  is the photon energy, and  $n$  refers to direct and indirect transitions. The calculation of absorption edge and optical absorption plays an essential role in the electronic structure study of amorphous material direct ( $n = \frac{1}{2}$ ) and indirect ( $n = 2$ ) (Davis and Mott 1970).

The Urbach energy  $E_u$  which is a character of disorder in the non-crystalline materials that can be indicated by a plot of  $\ln\alpha(\omega)$  of absorption coefficient  $\alpha(\omega)$  as a function of photon energy ( $\hbar\omega$ ) and determining the inverse of its slope, as described by this equation

$$\alpha(\omega) = B e^{\frac{\hbar\omega}{E_u}} \dots\dots 3.5$$

The refractive index ( $n$ ) can be calculated from the optical energy bandgap by using the equation below:

$$\frac{n^2-1}{n^2+2} = 1 - \sqrt{\frac{E_{opt}}{20}} \dots\dots 3.6$$

Synthesized glasses are found to be transparent. The optical band gap, direct and indirect and Urbach energy are listed in table (1).

The plots of  $(\alpha\hbar\omega)^{\frac{1}{2}}$  and  $(\alpha\hbar\omega)^2$  as a function of  $(\hbar\omega)$  for the (70-x)TeO<sub>2</sub>-30B<sub>2</sub>O<sub>3</sub>-xZnO (0= x ≥ 20 mol%) glass samples are shown in fig. (5) and fig. (6). The  $E_{opt}$  were calculated from the Tauc plots and are inserted in table (1). The values of optical band gap energy  $E_{dir}$  and  $E_{ind}$  are between (

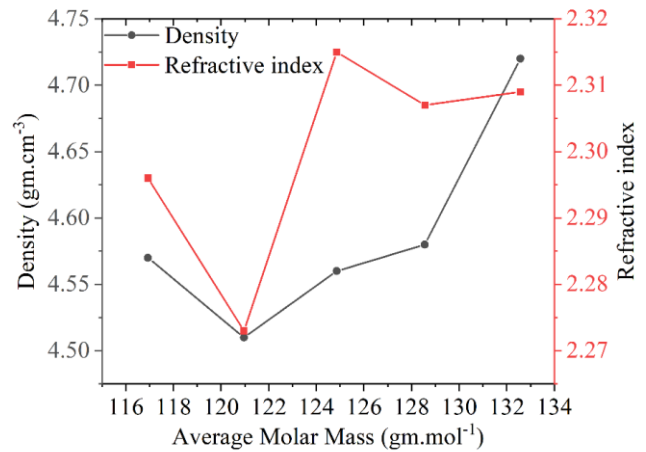


Fig. 4. The variation of density and refractive index with the average molar mass

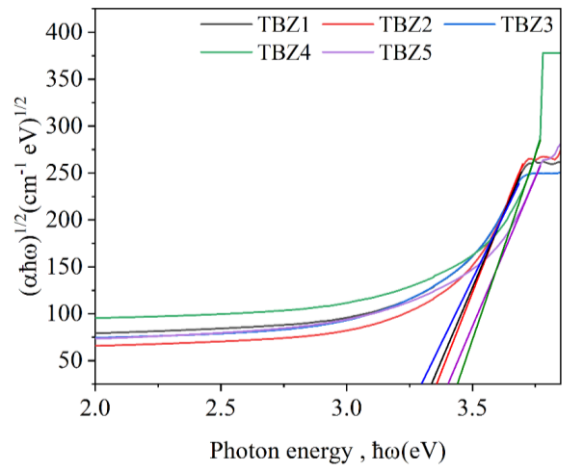


Fig. 5. Typical of indirect band gap for (70-x)TeO<sub>2</sub>-30B<sub>2</sub>O<sub>3</sub>-xZnO glass

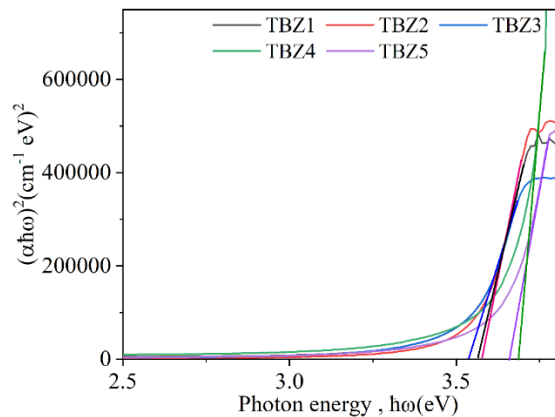


Fig. 6. Typical of direct band gap for (70-x)TeO<sub>2</sub>-30B<sub>2</sub>O<sub>3</sub>-xZnO glass

Using data from table (1), the plot of direct and indirect band gap energy versus ZnO

concentration are drawn and results in fig (7) for glass series. From fig. (7) it can be seen that the  $E_{ind}$  and  $E_{dir}$  increases as the ZnO is added up from 0 to 5 mol% and from 10 mol% to 15 mol% for indirect and direct band gap energy, respectively. This increase is due to the formation of more bridge oxygen. Then  $E_{ind}$  and  $E_{dir}$  are decrease as the ZnO content up from 5 mol% to 10 mol% and 15 mol% to 20 mol%. This decrement in the bandgap can be ascribed to an increase in the NBO due to the change in bonding with the addition of ZnO in the host glass network.

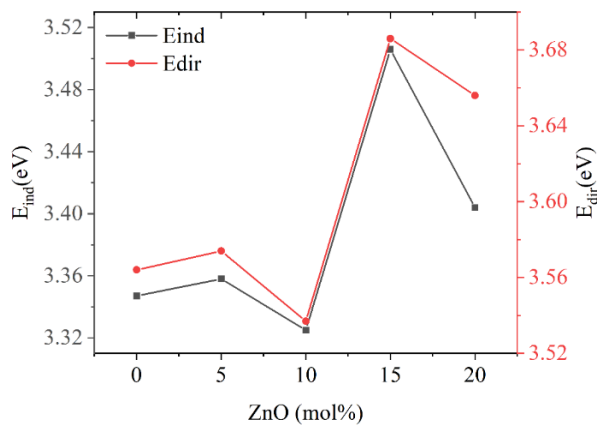


Fig. 7. Variation of direct and indirect energy bandgap with ZnO concentration

The plot of  $(\ln\alpha)$  against photon energy is shown in Figure (8), and it can be seen that the curve has a linear portion close to the edge of the band. The linear component shows an exponential behavior in the photon absorption process, which represents the emergence of a structural network flaw. The linear part's fitting and the Urbach tail behavior agree well. The Urbach energy values range from (0.17 eV-0.21 eV).

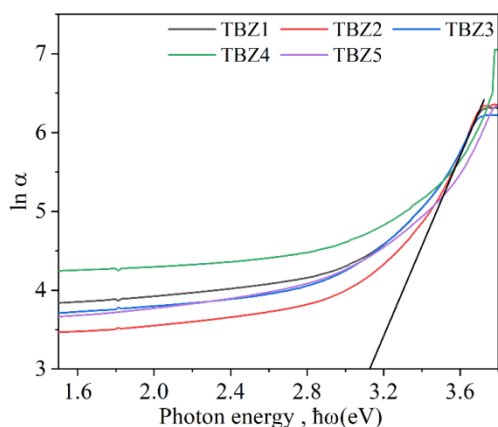


Fig. 8. Plot of  $\ln\alpha$  versus of Urbach energy of  $(70-x)\text{TeO}_2-30\text{B}_2\text{O}_3-x\text{ZnO}$  glass system

The linear part's inverse slope is used to estimate the Urbach energy. In the table, the Urbach energy is shown and listed in table (1). From Table (1), the variation of Urbach energy with ZnO concentration has been plotted and shown in figure (9). It is observed that Urbach energy decreased as the ZnO is added up from 0 to 5 mol% and from 10 mol% to 15 mol% which might be due to increment of local long-range order in the glassy system, thus causing the decrease in the width of the band tail. Urbach energy increases as the ZnO content increases from 5 mol% to 10 mol% and 15 mol% to 20 mol%; it is may be due to the rising of local short-range order.

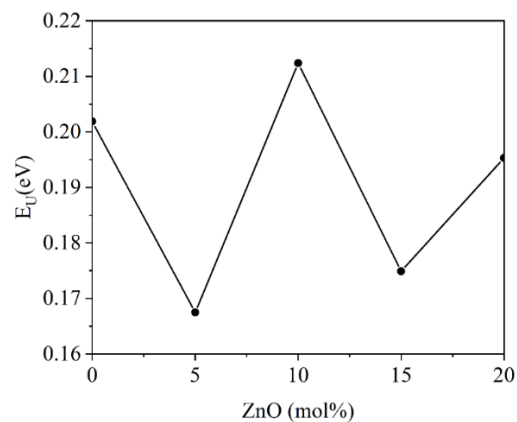


Fig. 9. The variation of Urbach energy with ZnO concentration

### 3.2 X-Ray Diffraction

The amorphous nature of the glass samples was analyzed and investigated using XRD analysis. The XRD patterns for the various compositions of  $(70-x)\text{TeO}_2-30\text{B}_2\text{O}_3-x\text{ZnO}$  glass are shown in fig (10). There is a broad humps in the range 20-35 degree which confirms the amorphous nature of the glass samples, which indicates the absence of periodicity of the three-dimensional network and the long-range atomic arrangement network in the sample. The lack of peaks in the figure is due to the amorphous structural formation in the glass samples. The absence of a sharp peak in the XRD pattern shows that there is no crystalline phase (Mawlud, Ameen et al. 2017).

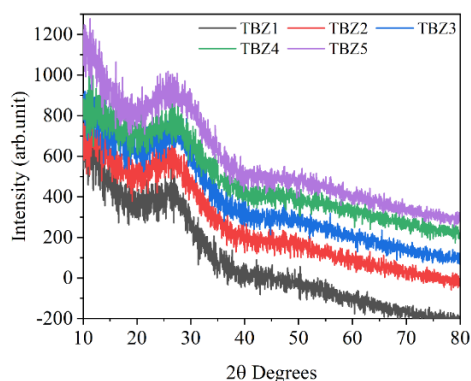


Fig. 10. Typical XRD pattern of glass with composition  $(70-x)TeO_2-30B_2O_3-xZnO$  ( $x = 0,5,10,15,20$ )

### 3.3 Fourier Transform Infrared

Fourier Transform Infrared (FTIR) spectroscopy is used to know about the structure change of the glass (Mawlud, Ameen et al. 2017). To study the functional group present in the amorphous glass samples, The plotted graph between transmittance against wavenumber had been take place. Fig (11) represents The FTIR spectra for various glass samples of borotellurite glasses doped with varying ZnO. The FTIR spectra of the prepared glass samples are recorded

in the range of  $400 - 4000\text{ cm}^{-1}$ . The range was used to study the fundamental vibration and associated rotational-vibration structure. Figure (11) provides detailed information for glass samples in this series concerning various bonding among different ions in the glass network. The identical peak assignments are listed in table (2), which summarizes the observed peaks in the entire spectral region and their corresponding band assignments for the glass sample in the series. For better clarity about the plot of FTIR spectra, we split the FTIR diagram into three separate regions:  $(400-1000\text{ cm}^{-1})$ ,  $(1000-2500\text{ cm}^{-1})$  and  $(2500-4000\text{ cm}^{-1})$ .

Figure (11a) show the appearance of the broad band around  $618.3-648.3\text{ cm}^{-1}$  and at  $761.3-768.5\text{ cm}^{-1}$  confirming the presence of stretching vibration mode between tellurium atom and bridging oxygen in the  $TeO_4$  and vibration of the  $TeO_3$  with non-bridging oxygen NBO, respectively. (Aziz, Sahar et al. 2018). In the third sample, the zinc wave number is around  $(410.8\text{ cm}^{-1})$  and for the TBZ5 sample it is around  $(417.6\text{ cm}^{-1})$ . It can be seen that for the TBZ1, TBZ2 and

Table.2. Infrared band position of  $(70-x)TeO_2-30B_2O_3-xZnO$  glass where  $x=0,5,10,15$  and 20 mol%

Sample code	ZnO (mol%)	Zn - O	$TeO_4$	$TeO_3$	$BO_4$	$BO_3$	H - O - H	Hydrogen Bonding	OH Group
TBZ 1	0	-----	635.3	768.5	998.0	1249.7	1636.4	2928.0	3451.7
TBZ 2	5	-----	629.9	764.0	993.5	1246.0	1609.2	2925.4	3432.5
TBZ 3	10	410.8	620.7	763.1	996.8	1263.0	1620.1	2926.7	3418.3
TBZ 4	15	-----	618.3	762.4	1000	1235.3	1630.1	2925.1	3446.1
TBZ 5	20	417.6	648.3	761.3	995.5	1266.7	1607.5	2927.8	3423.6

TBZ4 samples, the ZnO band does not appear in the spectra, which means that the zinc lattice is completely disrupted (Jambhale, Patil et al. 2017).

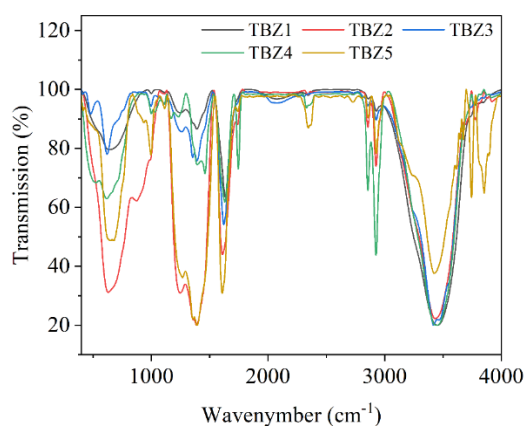


Fig. 11. FTIR spectra of  $(70-x)TeO_2-30B_2O_3-xZnO$  glass where  $x=0,5,10,15$  and 20 mol%

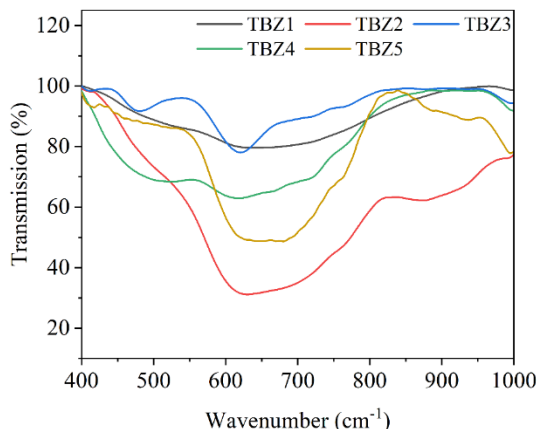


Fig. 11a. FTIR spectra of  $(70-x)\text{TeO}_2-30\text{B}_2\text{O}_3-x\text{ZnO}$  glass in the range of  $400-1000\text{ cm}^{-1}$

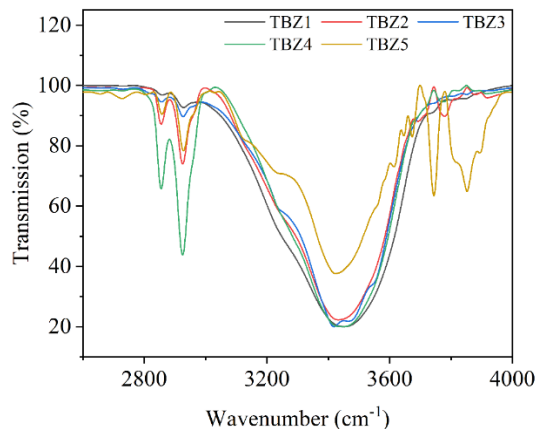


Fig. 11c. FTIR spectra of  $(70-x)\text{TeO}_2-30\text{B}_2\text{O}_3-x\text{ZnO}$  glass in the range of  $2600-4000\text{ cm}^{-1}$

Figure (11b) show the hydroxyl-metal (M-OH) stretching vibration bond for the glass. The bands were observed between  $1607.5-1636.4\text{ cm}^{-1}$  for TBZ glass group. Two observable broad bands recorded are at  $993.5-1000\text{ cm}^{-1}$  and  $1235.3-1266.7\text{ cm}^{-1}$  stretching of  $\text{BO}_4$  as well as asymmetric stretching of  $\text{BO}_3$  functional group, respectively (Faznny, Kamari et al. 2019).

The IR transmission bands occur around  $2900-3400\text{ cm}^{-1}$  belong to the stretching vibration of the hydroxyl bond. It is observed clearly for the series as shown in fig. (11c) the band ranges  $2925.1-2928.0\text{ cm}^{-1}$  and  $3418.3-3451.7\text{ cm}^{-1}$ , which correspond to hydrogen bond and hydroxyl bond, respectively.

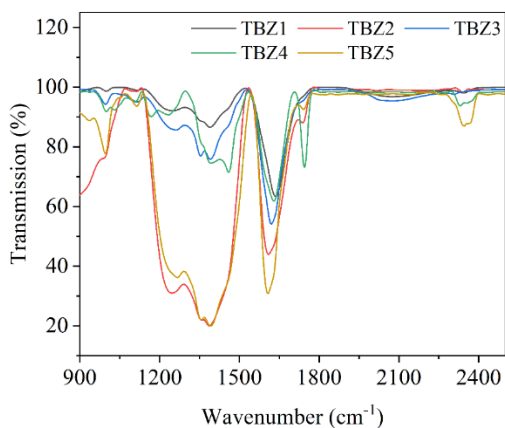


Fig. 11b. FTIR spectra  $(70-x)\text{TeO}_2-30\text{B}_2\text{O}_3-x\text{ZnO}$  glass in the range of  $900-2500\text{ cm}^{-1}$

#### 4. CONCLUSIONS

A transparent glass sample in the compositions  $(70-x)\text{TeO}_2-30\text{B}_2\text{O}_3-x\text{ZnO}$ , ( $0 = x \leq 20\text{ mol}\%$ ) has been prepared using the melt quenching technique. The role of increasing ZnO on the structural and optical properties of borotellurite glasses was studied by a conventional method. The density of the glass samples decreased when the ZnO mol% increased from 0 to 15 mol% as a result of an increase in NBO but when the ZnO mol% increased from 15 mol% to 20 mol% , the density of the glass samples increased due to the elevated BO rate. As the ZnO content increases 0 to 20 mol% then the molar volume decreases because the size of the ZnO molecular is smaller than the size of the borotellurite molecules so when we increase the zinc content it causes a decrease in the unit molar volume. the  $E_{\text{ind}}$  and  $E_{\text{dir}}$  increases as the ZnO is added up from 0 to 5 mol% and from 10 mol% to 15 mol% , while the Urbach energy is decreased due to the formation of more BO. Then  $E_{\text{ind}}$  and  $E_{\text{dir}}$  decrease as the ZnO content increases from 5 mol% to 10 mol% and 15 mol% to 20 mol% , while the Urbach energy increases due to the breakdown of BO and increased NBO content. The X-ray diffraction patterns didn't exhibit any intense peaks, indicating that the structure of the samples was amorphous in nature. FTIR results showed four prominent bands around  $(618.30-648.29\text{ cm}^{-1})$   $(761.28-768.53\text{ cm}^{-1})$  which are assigned to  $\text{TeO}_4$  and vibration of the  $\text{TeO}_3$ , and  $(993.48-1000.58\text{ cm}^{-1})$ ,  $(1235.33-1266.70\text{ cm}^{-1})$

represented to  $\text{BO}_4$  as well as asymmetric stretching of  $\text{BO}_3$ .

### Acknowledgements

The author gratefully acknowledges the financial support from Ministry of Higher Education, and University of Salahaddin/Ministry of Higher Education/KRG

### References

- Ahmed, K. F., et al. (2017). "Effect of Rare Earth Co-Doping On Physical and Optical Characterization of Zinc Tellurite Glass Embedded Ag NPs." **28**(6): 68-73.
- Ardelean, I., et al. (2007). "EPR and magnetic susceptibility studies of manganese ions in  $70\text{TeO}_2 \cdot 25\text{B}_2\text{O}_3 \cdot 5\text{SrO}$  glass matrix." **101**(1): 177-181.
- Aziz, S. M., et al. (2018). "Spectral attributes of  $\text{Eu}^{3+}$  doped borotellurite glasses containing  $\text{Mn}_3\text{O}_4$  nanoparticles." **735**: 1119-1130.
- Davis, E. and N. J. P. m. Mott (1970). "Conduction in non-crystalline systems V. Conductivity, optical absorption and photoconductivity in amorphous semiconductors." **22**(179): 0903-0922.
- El-Falaky, G. E., et al. (2012). "AC conductivity and relaxation dynamics in zinc-borate glasses." **22**(2): 86-93.
- El-Mallawany, R. (2018). Tellurite glass smart materials: applications in optics and beyond, Springer.
- Faznny, M., et al. (2019). Optical properties of  $\text{La}^{3+}$  NPs/Ag+ Co-doped zinc borotellurite glass. Solid State Phenomena, Trans Tech Publ.
- Gautam, C. and A. K. Yadav (2013). "Synthesis and optical investigations on (Ba, Sr)  $\text{TiO}_3$  borosilicate glasses doped with  $\text{La}_2\text{O}_3$ ."
- Halimah, M., et al. (2019). "Study of rice husk silicate effects on the elastic, physical and structural properties of borotellurite glasses." **238**: 121891.
- Hasnimulyati, L., et al. (2016). Elastic properties of thulium doped zinc borotellurite glass. Materials Science Forum, Trans Tech Publ.
- Jambhale, V. N., et al. (2017). "FT-IR and Density Studies on Neodymium Doped Zinc Borotellurite Glass System." **7**: 562-565.
- Kaur, A., et al. (2010). "Preparation and characterization of lead and zinc tellurite glasses." **356**(18-19): 864-872.
- Kumari, S., et al. (2021). "Nonlinear optical characterization of zinc doped tellurite glasses for optical limiting performance." **228**: 166193.
- Pavani, P. G., et al. (2011). "Optical, physical and structural studies of boro-zinc tellurite glasses." **406**(6-7): 1242-1247.
- Kundu, R., et al. (2014). "Bismuth modified physical, structural and optical properties of mid-IR transparent zinc boro-tellurite glasses." **587**: 66-73.
- Mawlud, S. Q. (2018). Optical Properties of Tellurite Glasses Embedded with Gold Nanoparticles. Tellurite Glass Smart Materials, Springer: 105-142.
- Mawlud, S. Q., et al. (2017). "Spectroscopic properties of  $\text{Sm}^{3+}$  doped sodium-tellurite glasses: Judd-Ofelt analysis." **69**: 318-327.
- Mawlud, S. Q., et al. (2017). "Structural and thermal behavior of  $\text{Sm}^{3+}$  ions doped sodium tellurite glasses." **29**(2).
- Mawlud, S. Q. J. J. o. L. (2021). "Physical and thermal properties of gold nanoparticles embedded  $\text{Nd}^{3+}$ -doped borophosphate glasses: Spectroscopic parameters." **236**: 118079.
- Mekki, A., et al. (2005). "Structural and magnetic properties of  $\text{MoO}_3\text{-TeO}_2$  glasses." **351**(30-32): 2493-2500.
- Pavani, P. G., et al. (2011). "Optical, physical and structural studies of boro-zinc tellurite glasses." **406**(6-7): 1242-1247.
- Saddeek, Y. B., et al. (2009). "Physical and structural properties of some bismuth borate glasses." **115**(1): 280-286.
- Sharma, B. I., et al. (2004). "Study on some thermo-physical properties in  $\text{Li}_2\text{O-ZnO-SiO}_2$  glass-ceramics." **58**(19): 2423-2428.
- Sidek, H., et al. (2009). "Synthesis and optical properties of  $\text{ZnO-TeO}_2$  glass system." **6**(8): 1489.